Chapter 2
Power Converters for Small- to Large-Scale Photovoltaic Power Plants

Abstract This chapter presents an extensive literature survey on various different aspects of medium-voltage (MV) converter development for step-up-transformer-less direct grid integration of photovoltaic (PV) power plants. The main objective was to show how power electronic converter topologies, power electronic devices, and control complexities have affected the development of the MV converter and how to make an excellent choice of the converter topology for step-up-transformer-less grid integration through the MV converter. Besides the traditional system, which requires a step-up transformer to connect the renewable power plants to the grids, other recently proposed converter topologies for step-up-transformer-less direct grid interconnection are also introduced in detail with the aim of presenting a complete picture of power converter topologies for small- to large-scale PV power plants.

Keywords Power converters · Photovoltaic inverters · Small to large scale · Power plants · Remote area · Medium voltage

2.1 Introduction

The world's energy demand is growing remarkably due to the fast growth of population and economy in the developing countries. The energy sector is facing an accelerating amalgam crisis of the worldwide established fossil and atomic energy systems. Natural gas, coal, and crude oil are the main fossil fuels for the current world energy supply. Crude oil is the most important fossil fuel among the three main fossil flues. Figure 2.1 shows the trend of world oil consumption [1]. Coal is the second most important consumable fossil fuel. Figure 2.2 shows the world coal consumption [1]. Due to very high oil price, coal has been becoming an attractive fossil fuel in the recent years. Figure 2.3 shows the world consumption of natural gas [1]. Almost a constant growth rate has been observed for the natural gas consumption in the past decades.

M.R. Islam et al., *Power Converters for Medium Voltage Networks*,
Green Energy and Technology, DOI 10.1007/978-3-662-44529-7_2

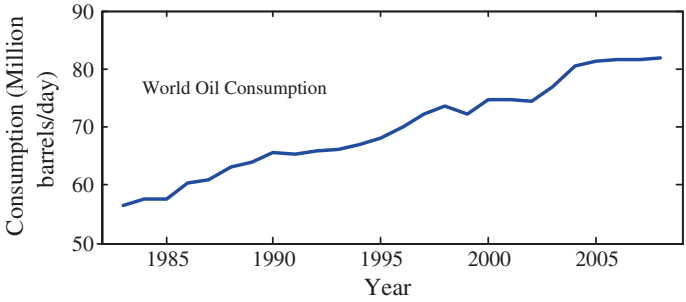

Fig. 2.1 World oil consumption [1]

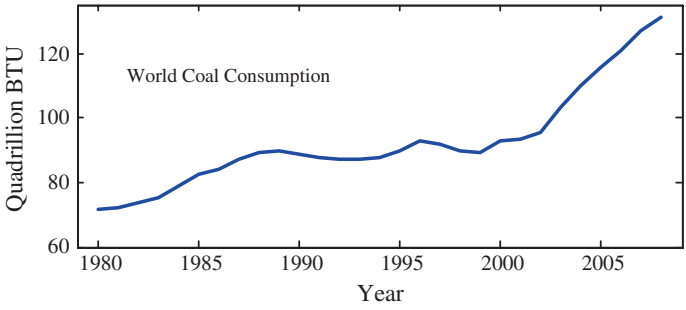

Fig. 2.2 World coal consumption [1]

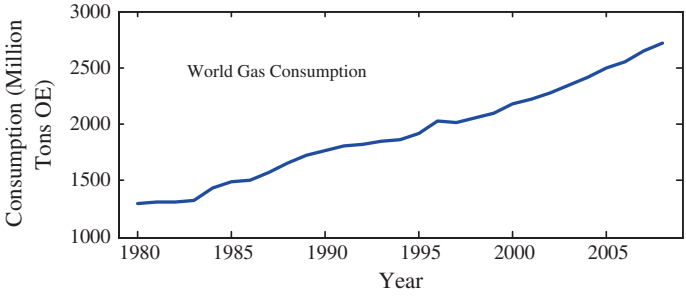

Fig. 2.3 World natural gas consumption [1]

The increasing energy demand is not only diminishing the reserve of fossil fuels, but also affecting the environment. Carbon dioxide (CO_2) gas is generated from burning of fossil fuels, which significantly contributes to the increase of average global temperatures, i.e., global warming. Figure 2.4 shows the world CO_2 emission from fossil fuel burning [1]. Scientists worldwide are now seeking

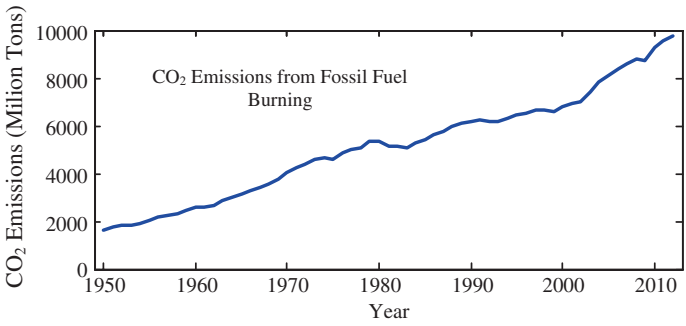

Fig. 2.4 World CO_2 emission form fossil fuel burning [1]

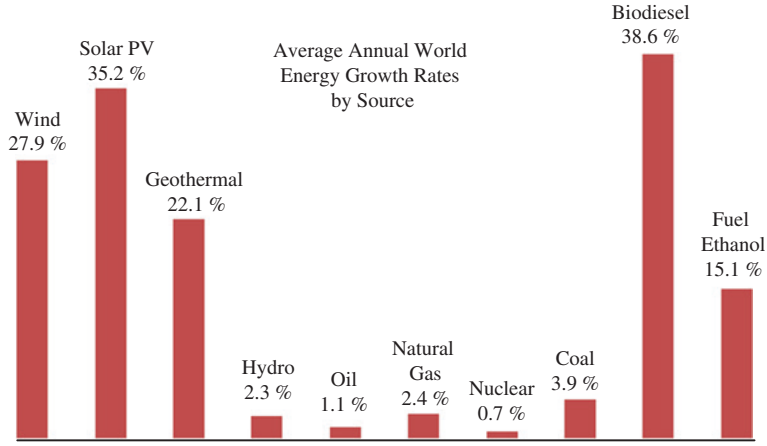

Fig. 2.5 Average annual world energy growth rates by source [1]

solutions to these two enormous challenges (energy and environment) from renewable or clean energy sources, which are richly available in almost every country.

Many countries have set targets for renewable energy use to meet the increasing energy demand and also to reduce the global warming effect. For example, the target shares of total energy from renewables by 2020 in Sweden, Finland, Austria, and Australia are 49, 38, 34, and 20 %, respectively [2]. Therefore, average annual growth rates of renewable sources are much higher than those of conventional sources in recent years. Figure 2.5 shows the average annual world energy growth rates [1]. Solar photovoltaic (PV) represents the second highest growth rate due to its abundance source and technological development of PV cell, e.g., reduction of PV module cost. Average module cost was USD 100/W and USD 29/W in 1975 and 1980, respectively, and reduced to less than USD 3.5/W in 2004. Figure 2.6 shows the average PV module cost [1].

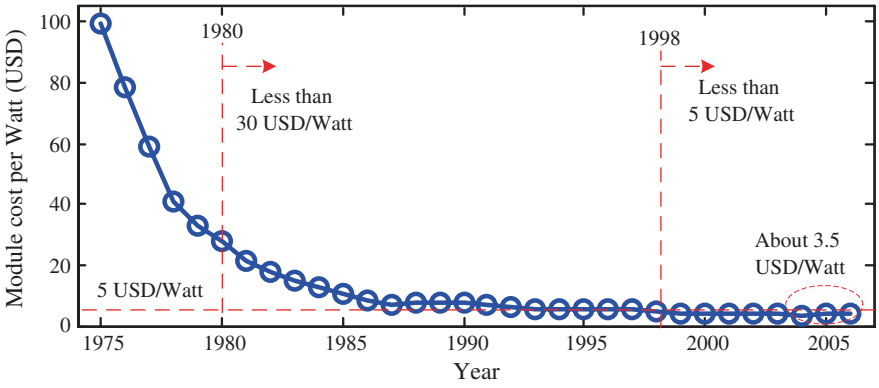

Fig. 2.6 Average photovoltaic module cost [1]

Since 2007, medium- and large-scale PV power plants have attracted a high degree of attention and the power plants of more than 10 MW in capacity have now become a reality. These multi-megawatt PV power plants require large areas of land, and thus, they are usually installed in remote areas, far from cities. For power transmission, a step-up transformer is usually used in the PV inverter system to feed in the solar energy into a medium-voltage (MV) grid (e.g., 6–36 kV). The transformer steps up the inverter output voltage from 300 V AC to grid voltage level (e.g., 6–36 kV). Although these special transformers are compact compared with conventional distribution transformers, they are still large and heavy for remote area PV applications. The large-size and heavy weight step-up transformer may increase the system weight and volume and can be expensive and complex for installation and maintenance. The MV inverter may offer the best possible solution to interconnect the PV array to the MV grid directly [3]. Moreover, it may also be possible to ensure electrical isolation through the inverter, which is important for the interconnection of MV grid and PV array [4]. Recently, advanced magnetic materials, such as amorphous and nanocrystalline alloys, have attracted significant attention to develop high-frequency magnetic links for MV inverters [5]. Compared with the power frequency transformer (operated at 50/60 Hz), the high-frequency magnetic links (in the range of a few kHz–MHz) have much smaller and lighter magnetic cores and windings and thus much lower cost. Therefore, the MV inverter for step-up-transformer-less direct grid interconnection of PV systems has become a favorable choice, since the installation of large-scale PV power plants started commercially in 2007.

This chapter incorporates PV power generation technologies, including traditional power conditioning systems, two-level low-voltage converter topologies, the limitations of power frequency step-up transformer-based grid integration of renewable generation systems in remote area applications, and advanced converter topologies for MV applications. Therefore, an extensive literature survey has been conducted focusing on many different aspects of MV converter development for

step-up-transformer-less direct grid integration of PV power generation systems. The main objective of this general review on power electronic converter topologies is to show how topologies, power electronic devices, and control complexities have affected the development of the MV converter and to understand which converter topology would be a natural choice for step-up-transformer-less grid integration through the MV converter.

2.2 Solar Photovoltaic Arrays

The "solar photovoltaic" means "producing electricity from sunlight." A PV cell can be made by two semiconductor layers; one having positive charge and the other having negative charge. When the sunlight shines on a PV cell, some of the photons from the sunlight are absorbed by the semiconductor atoms, releasing electrons from the cell's negative layer. If there is an external circuit, the free electrons flow to the positive layer and produce electric current in the external circuit. Figure 2.7 shows a photograph of PV cell.

One silicon PV cell can produce about 0.5 V, which is too small to do valuable work. To increase the voltage, several individual PV cells are interconnected together in package called a module. For example, a 12-V module will have 36 individual cells connected in series. In 24 V applications, two 12-V modules can be connected in series, where the current stays unchanged. Figure 2.8 shows a photograph of 24-V PV module. Table 2.1 summarizes the electrical characteristics of solar module SX-10. When two modules are wired in parallel, their current is doubled and the voltage stays unchanged. To achieve the desired voltage and current,

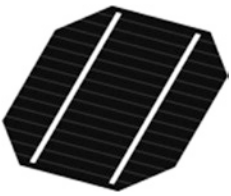

Fig. 2.7 A photograph of PV cell, which may produce 0.5 V DC

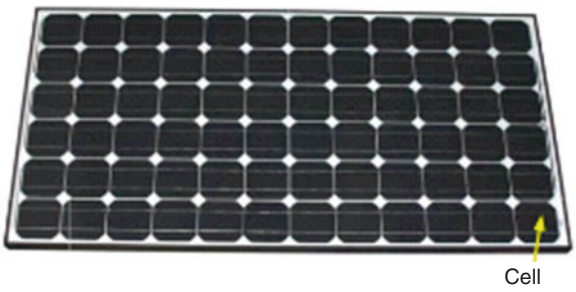

Fig. 2.8 A photograph of 24-V PV module, where 72 cells are interconnected

Table 2.1 Electrical characteristics of solar module SX-10

Parameters	Rating
Nominal voltage	12 V
Rated power	10 W
Number of PV cells	36 (connected in series)
Voltage at P_{max} (V_{mp})	16.8 V
Current at P_{max} (I_{mp})	0.59 A
Short-circuit current (I_{sc})	0.65 A
Open-circuit voltage (V_{oc})	21.0 V
Temperature coefficient of I_{sc}	(0.065 ± 0.015) %/°C
Temperature coefficient of V_{oc}	$-(80 \pm 10)$ mV/°C
Temperature coefficient of power	$-(0.5 \pm 0.05)$ %/°C

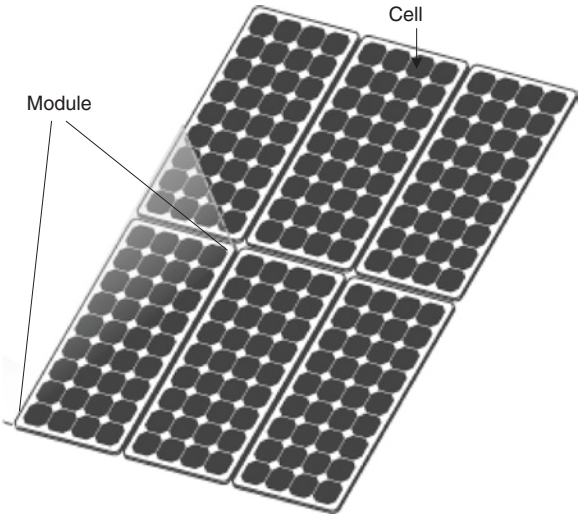

Fig. 2.9 A photograph of PV array with six 12-V modules, where 36 cells are interconnected in each module

a number of modules can be connected in series and parallel. The series–parallel combination of modules is called a PV array. Figure 2.9 shows a photograph of PV array with six 12-V modules, where 36 cells are interconnected in each module.

2.2.1 Solar Photovoltaic Array Modeling

When PV arrays are used to harvest solar energy, two important factors could limit the implementation of PV systems, i.e., high cost and low efficiency in energy conversion. The conversion efficiency of the current solar PV modules is typically only about 10–17 % [6]. In PV systems, the PV array represents about 57 % of the total cost of the system, and the battery storage system corresponds to 30 % of the cost. Other system components such as inverters and maximum power point tracker (MPPT) contribute to only 7 % of the total cost [7]. Due to the low

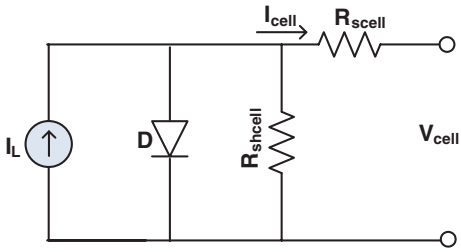

Fig. 2.10 Equivalent circuit of a PV cell

conversion efficiency and high cost of solar array, it is very desirable to operate the PV panel at the maximum power point (MPP). An ideal solar cell can be modeled by a current source in parallel with a diode. In practice, no solar cell is ideal and hence a shunt resistance and a series resistance are added to the model as shown in Fig. 2.10, where R_{scell} is the intrinsic series resistance of usually a very small value, and R_{shcell} is the equivalent shunt resistance of usually a very large value.

For a single silicon solar cell, the nonlinear *I–V* characteristic can be presented as [8, 9]

$$I_{\text{cell}} = I_{\text{L}} - I_{\text{o}}\left[\exp\left(G(V_{\text{cell}} + I_{\text{cell}}R_{\text{scell}})\right) - 1\right] - \frac{V_{\text{cell}} + I_{\text{cell}}R_{\text{scell}}}{R_{\text{shcell}}} \tag{2.1}$$

where
$G = \frac{q}{A_i KT}$,

q is the electronic charge ($=1.602 \times 10^{-19}$ C),
$A_i = B_i$ is the ideality factor ($=1.92$),
K is the Boltzmann's constant ($=1.38 \times 10^{-23}$ J/K),
T is the PV cell temperature,
I_{cell} is the cell output current,
V_{cell} is the cell output voltage,
I_{o} is the cell saturation current which can be presented as

$$I_{\text{o}} = I_{\text{or}}\left(\frac{T}{T_{\text{r}}}\right)^3 \exp\left[\frac{qE_{\text{GO}}}{B_i K}\left(\frac{1}{T_{\text{r}}} - \frac{1}{T}\right)\right] \tag{2.2}$$

I_{L} is the light-generated current which can be presented as

$$I_{\text{L}} = \left[I_{\text{SC}} + K_{I_{\text{SC}}}(T_C - 28)\right] \times \frac{R_{\text{ad}}}{1{,}000} \tag{2.3}$$

The array temperature T_{c} is approximately given by [9]

$$T_{\text{C}} = T_{\text{air}} + 0.3 \times R_{\text{ad}}\ \% \tag{2.4}$$

T_{r} is the reference temperature ($=301$ K),
I_{or} is the reverse saturation current at T_{r} ($=19.9693 \times 10^{-6}$ A),
I_{os} is the cell reverse saturation current, A
T_{c} is the cell temperature, °C
$K_{I\text{sc}}$ is the short-circuit current temperature coefficient ($=0.0017$ A/°C)

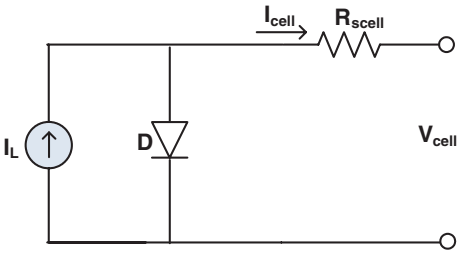

Fig. 2.11 Simplified equivalent circuit of a PV cell

R_{ad} is the cell illumination, W/m^2 (1,000 W/m^2 = 100 % illumination)
I_{sc} is the cell short-circuit current at 28 °C and 1,000 W/m^2 (=2.52 A)
EG_o is the band gap for silicon (=1.11 eV)
T_{air} is the ambient temperature, °C

Since PV arrays are built up with series and/or parallel connected combinations of solar PV cells, for an array with $n_S \times n_P$ cells, the current equation can be presented as [9, 10]

$$I_{PV} = n_p I_L - n_p I_o \left[\exp\left(G\left(\frac{V_{PV} + I_{PV}R_s}{n_s}\right)\right) - 1\right] - \frac{V_{PV} + I_{PV}R_s}{R_{sh}}. \quad (2.5)$$

where
$I_{PV} = n_P I_{cell}$ is the PV array output current,
$V_{PV} = n_S V_{cell}$ is the PV array output voltage,
n_s is the number of cells connected in series,
n_p is the number of panels connected in parallel,
$R_S = R_{Scell}\frac{n_S}{n_P}$ is the PV array series resistance, and
$R_{sh} = R_{shcell}\frac{n_S}{n_P}$ is the PV array shunt resistance.

The shunt resistance R_{shcell} is much greater than the series resistance R_{scell}, which makes the last term of (2.1) much smaller than the other terms. The simplified cell equivalent circuit is shown in Fig. 2.11.

The current–voltage relation of simplified PV cell can be expressed as

$$I_{cell} = I_L - I_o\left[\exp\left(G(V_{cell} + I_{cell}R_{scell})\right) - 1\right] \quad (2.6)$$

and the array current–voltage relation becomes

$$I_{PV} = n_p I_L - n_p I_o \left[\exp\left(G\left(\frac{V_{PV} + I_{PV}R_s}{n_s}\right)\right) - 1\right]. \quad (2.7)$$

2.2.2 Solar Photovoltaic Array Characteristics

Solar energy sources have variable daily and seasonal patterns. For example, monthly average global solar insolation at Dhaka City of Bangladesh varies between 3.92 and 7.71 kW h/m^2/day. The maximum amount of insolation

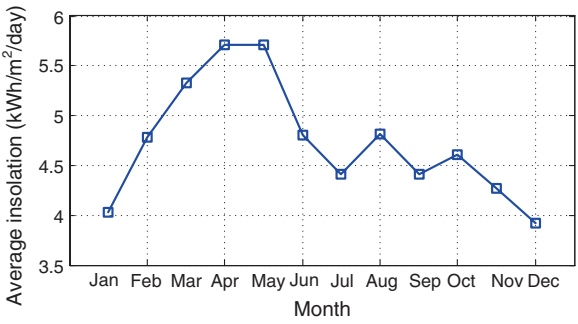

Fig. 2.12 Monthly average global solar insolation at Dhaka City of Bangladesh; recording period: 1988–1998 [11]

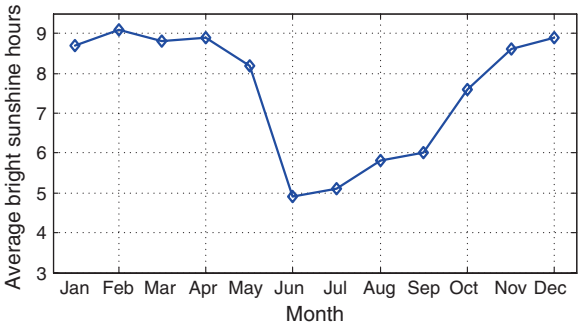

Fig. 2.13 Daily average bright sunshine hour at Dhaka City of Bangladesh; recording period: 1961–1980 [11]

is available in the months of March–May, and the minimum in December–January. Figure 2.12 shows the monthly global solar insolation at Dhaka City of Bangladesh [11]. Daily bright sunshine hours have also variable daily and seasonal patterns. For example, the daily average bright sunshine hour at Dhaka City of Bangladesh vary between 4.9 and 9.1 h. The maximum is in the months of February–April, and the minimum is in the June–September. Figure 2.13 shows the daily average bright sunshine hours at Dhaka City of Bangladesh [11]. The output characteristics of the PV array are nonlinear and critically affected by the solar radiation, temperature, and load conditions. The current versus voltage (*I–V*) and power versus voltage (*P–V*) characteristics with various irradiances at 25 °C temperature are shown in Figs. 2.14 and 2.15, respectively [12, 13]. The simulated *I–V* and *P–V* characteristics with various temperatures at 1,000 W/m^2 irradiance are illustrated in Figs. 2.16 and 2.17, respectively [12, 13].

2.2.3 Solar Photovoltaic Array Maximum Power Point

It is also observed from the power–voltage curve of the solar PV module that on the right hand side, when the voltage is almost constant, the slope of power versus

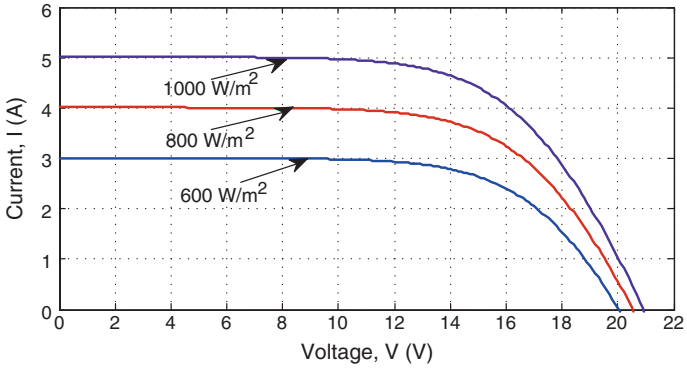

Fig. 2.14 Calculated *I–V* curves at different irradiance ranging from 600 to 1,000 W/m^2; 25 °C temperature was considered for the calculation [12, 13]

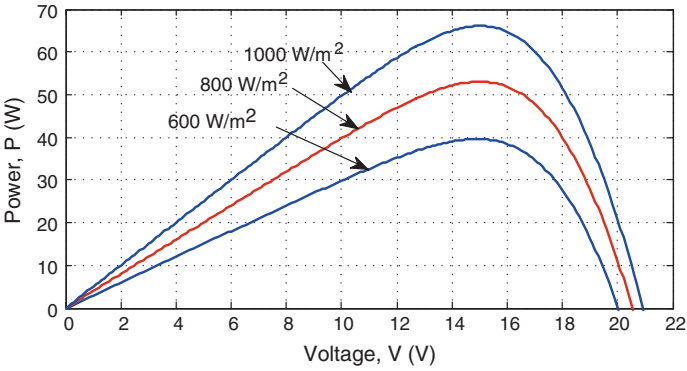

Fig. 2.15 Calculated *P–V* curves at different irradiance ranging from 600 to 1,000 W/m^2; 25 °C temperature was considered for the calculation [12, 13]

voltage is negative ($\Delta P/\Delta V < 0$), whereas on the left hand side, the slope is positive ($\Delta P/\Delta V > 0$), as illustrated in Fig. 2.18 [12, 13]. Thus, the PV array has an optimum operating point called the MPP, which varies depending on array temperature and the present insolation level. The irradiance mainly affects the output current, and the temperature mainly affects the terminal voltage of the PV array, so that the effects of both factors have to be considered when designing a PV system. However, the intermittent nature of PV sources, in terms of the power and output voltage, is a major issue when connected to the grid. Therefore, solar PV system requires a power conditioning circuit known as PV inverter that is capable of extracting the maximum power from PV source and feeds the adjusted power to the load and/or grid to their satisfaction.

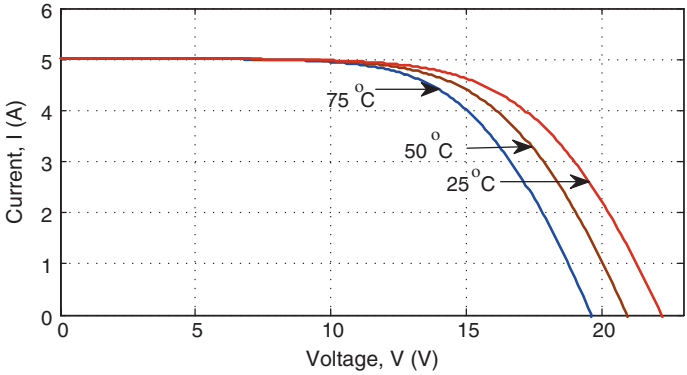

Fig. 2.16 Calculated *I–V* curves at different temperature ranging from 25 to 75 °C; irradiance 1,000 W/m^2 was considered for the calculation [12, 13]

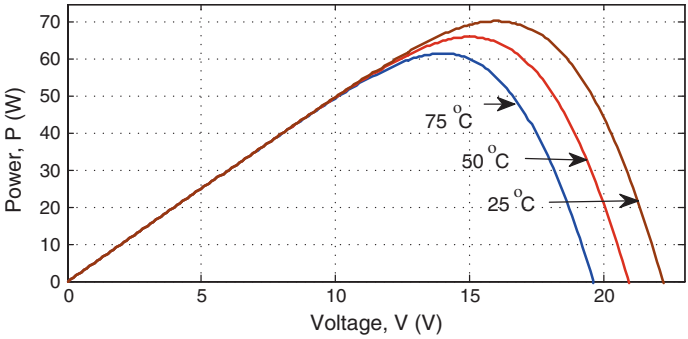

Fig. 2.17 Calculated *P–V* curves at different temperature ranging from 25 to 75 °C; irradiance 1,000 W/m^2 was considered for the calculation [12, 13]

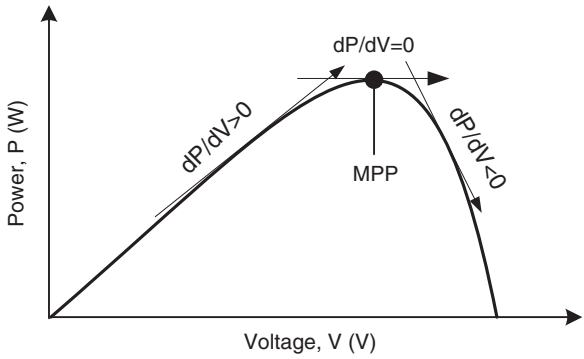

Fig. 2.18 Maximum power point (*MPP*) determination: The slope is positive on the left side of the *P–V* curve, negative on the right side, and zero at the MPP [12, 13]

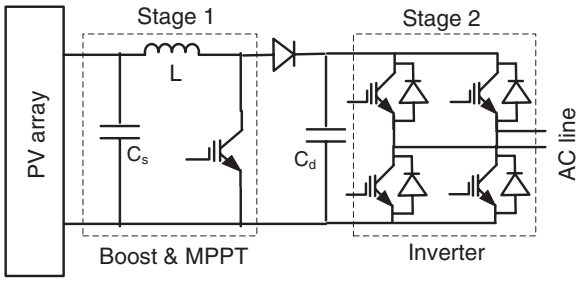

Fig. 2.19 Fundamental circuit of two-stage PV inverter [14]

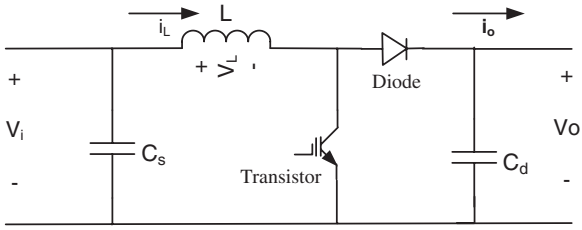

Fig. 2.20 Most commonly used DC to DC boost converter circuit

2.3 Inverters in Small-Scale Solar PV Systems

2.3.1 Two-Stage Solar PV Inverters for Small-Scale Systems

Usually, a PV inverter has two stages to shape the PV array output power for feeding into the AC load. The first stage is responsible for boosting the PV array voltage and tracking the MPP, and the second stage inverts available DC power into AC power. The most fundamental circuit topology of the two-stage PV inverter using the full-bridge as shown in Fig. 2.19 was proposed in [14].

Usually, the source-side controller tracks the maximum power and the load-side controller controls the power factor of output current and maintains constant DC voltage across capacitor C_d. When the transistor is turned on, the energy from PV array is stored in the inductor L. When transistor is turned off, the inductor stored energy is delivered to the DC-link capacitor C_d and the H-bridge inverter. The booster circuit can have two distinct modes of operation, the continuous current conduction and discontinuous current conduction, of significantly different characteristics. The booster circuit, as shown in Fig. 2.20, is also known as the step-up DC to DC converter; its typical application is to convert low input voltage to a high output voltage. When the transistor is turned on, the source voltage V_i is applied across the inductor and the rising rate of inductor current is dependent on the source voltage V_i and inductance L. Figure 2.21 shows the equivalent circuit of the DC to DC boost converter when the transistor is turned on.

When the transistor is turned off, the equivalent circuit is shown in Fig. 2.22 and the inductor voltage becomes

$$v_L = V_i - V_o \tag{2.8}$$

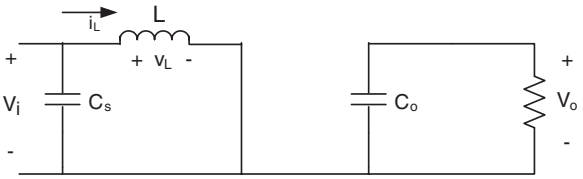

Fig. 2.21 Equivalent circuit of a DC to DC boost converter when transistor is turned on

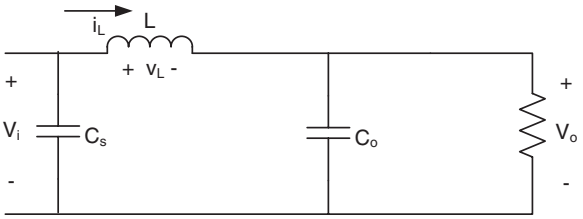

Fig. 2.22 Equivalent circuit of a DC to DC boost converter when the transistor is turned off

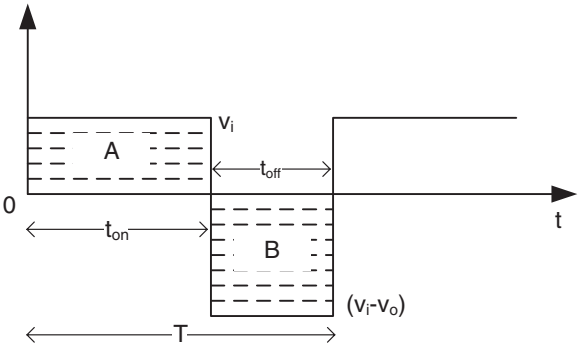

Fig. 2.23 Voltage across inductor L for time period T

For steady-state operation, the integral of inductor voltage v_L over one time period T must be zero, i.e., the areas A and B in Fig. 2.23 must be equal.

Therefore,

$$V_i \times t_{on} + (V_i - V_o) \times t_{off} = 0 \tag{2.9}$$

Dividing both sides by T, and rearranging all terms, we have

$$\frac{V_o}{V_i} = \frac{T}{t_{off}} = \frac{1}{1-D} \tag{2.10}$$

Assuming the circuit is 100 % efficient, i.e., the input power (P_i) and output power (P_o) are equal, ($P_i = P_o$), or

$$V_i \times I_i = V_o \times I_o \tag{2.11}$$

one obtains

$$\frac{I_o}{I_i} = (1-D) \tag{2.12}$$

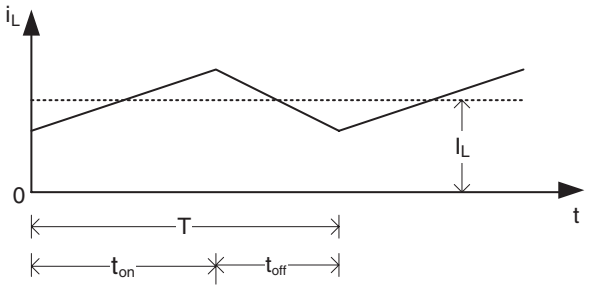

Fig. 24 Waveform of inductor current in the continuous conduction mode

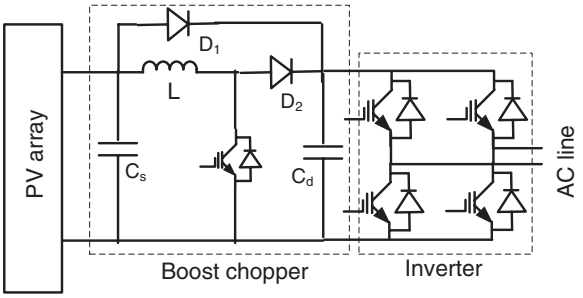

Fig. 2.25 Time-sharing chopper-based-modified circuit of two-stage PV inverter

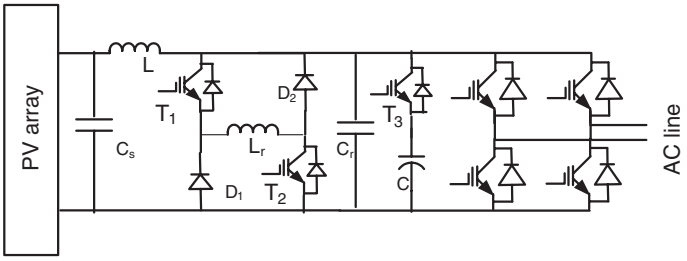

Fig. 2.26 Parallel resonant DC-link-based-modified two-stage PV inverter circuit

In the continuous operation mode, the inductor current never falls to zero in one switching cycle, i.e., either the transistor or diode is conducting. Figure 2.24 shows the inductor current in the continuous conduction mode.

Several modified topologies, such as a time-sharing dual-mode PV inverter [15] in Fig. 2.25 and a soft-switched DC to DC boost converter-based inverter [16] in Fig. 2.26, were proposed to improve the efficiency of the fundamental circuit. In the time-sharing dual-mode PV inverter, when the PV array output voltage is larger than the DC-link voltage, the transistor is always in the off state and the input current flows through the bypass diode D_1 but does not flow through the boost inductor

L and free-wheeling diode D_2. In this way, the proposed circuit can avoid the conduction losses of boost inductor, L, and the free-wheeling diode D_2. When the input voltage is smaller than the DC-link voltage, the bypass diode D_1 behaves as open circuit and the circuit operates as a fundamental two-stage PV inverter circuit. In the soft-switched DC to DC boost converter-based PV inverter, there are two stages: the converter stage and inverter stage. All the switches in both the converter and inverter stages can be turned on and off with zero voltage switching, which can reduce the switching losses significantly. The operating principle of the proposed soft switching inverter was presented with a few switching modes [16] as the following:

Mode 1 When the transistor in DC-link capacitor C is turned on with zero voltage switching, the DC-link capacitor begins to discharge and linearly decreases the main inductor L current.

Mode 2 When the transistors T_1, T_2, and T_3 are turned on with zero voltage switching, the DC-link capacitor begins to discharge.

Mode 3 When T_1 and T_2 are turned on with zero voltage switching, the resonance between resonance inductor, L_r, and resonance capacitor, C_r, is started and the main inductor current is minimized. When the resonance is finished, the current of resonant inductor, L_r, flows through diodes, D_1 and D_2.

Mode 4 When T_1 and T_2 are turned off with zero voltage switching, resonance is started. The resonant capacitor C_r is charged by the current flowing through inductors, L and L_r. The resonance stops when the voltage of resonant capacitor, C_r, equals the output voltage. The DC-link capacitor is charged by L and L_r through the parallel diode of T_3.

2.3.2 Multiple-Stages Solar PV Inverters for Small-Scale Systems

Due to the high value of stray capacitance of PV array, a galvanic connection between the ground of the grid and the PV array may exist. In this case, dangerous leakage current called common-mode current may appear through the stray capacitance between the PV array and the ground. The capacitance between PV cells and the ground can reach very high value under certain conditions, such as the PV array structure, and weather there are humidity and dust covering the PV array. This capacitance can reach up to 150 nF/kWp for crystalline-silicon cells and 1 μF/kWp for thin-film cells. The common-mode leakage current may increase the system power loss, reduce the grid current quality, and cause personnel safety problems [17, 18]. Therefore, galvanic isolation is essential because it permits easy array grounding, array isolation from grid in case of fault, and safety of personnel, and can strongly reduce the leakage current between the PV array and the ground. The connection of grid neutral and middle points of the DC link is one of the options to reduce the ground leakage currents. In this context, Rahman and Zhong [19] proposed a half-bridge topology-based PV inverter as shown in Fig. 2.27. The step-up

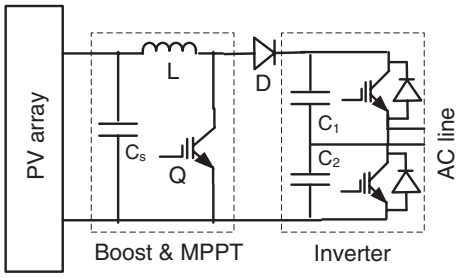

Fig. 2.27 Basic circuit of half-bridge topology-based PV inverter

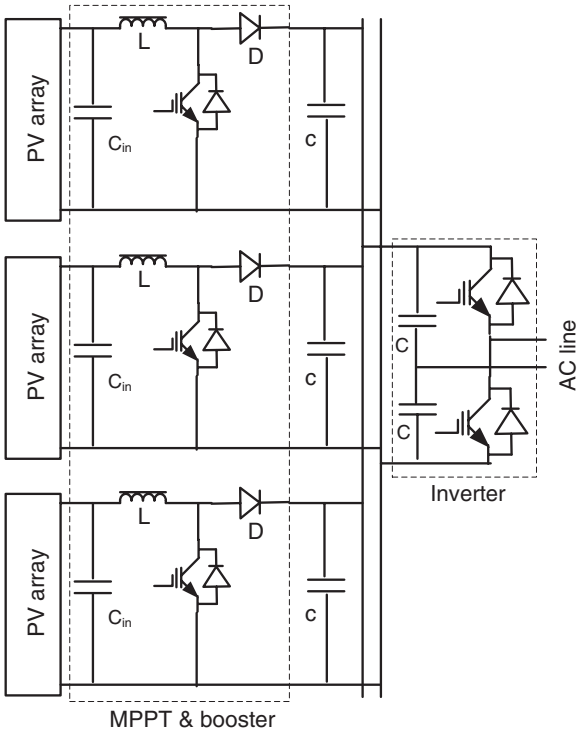

Fig. 2.28 Sunny Boy 5000TL model half-bridge topology-based PV inverter

(boost) converter raises the voltage of the PV array and also serves the operation of MPPT. Driven by the proper reference signals generated by the control algorithm to modulate the pulse width of the switching signal of switch Q, the half-bridge inverter inverts the DC power to 50 or 60 Hz AC power. Figure 2.28 illustrates the half-bridge topology-based three-string PV inverter, Sunny Boy 5000TL, commercially developed by SMA [20]. The half-bridge inverter-based topology requires less switching devices, but its DC-link voltage needs to be twice the grid voltage peak. The inverter topologies do not have electrical isolation between the array and the grid, which is critical in case of fault and safety of personnel.

The insulation can be achieved through a power frequency transformer at the grid side of the PV inverter which may also serve voltage step-up operation.

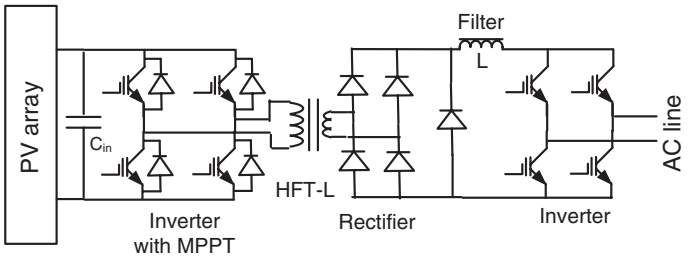

Fig. 2.29 High-frequency transformer-link (*HFT-L*)-based PV inverter power circuit

This power frequency transformer is heavy and large, increasing the PV inverter installation cost and requiring regular monitoring and maintenance. Increasing the operating frequency will lead to a compact and lightweight magnetic component of isolation transformers [4, 5, 21]. Several medium- and high-frequency (HF) transformer-based inverter topologies were developed and made available commercially. Figure 2.29 shows a high-frequency link-based inverter system [10]. The DC PV array power is converted to 50 or 60 Hz AC line power through an isolated high-frequency transformer link. The DC voltage of the PV array is firstly converted to high-frequency AC by a high-frequency inverter, which is then transformer-coupled and converted to 50 or 60 Hz AC through a high-frequency rectifier, filter, and a full-bridge inverter. The multistage power conversion may increase the cost of the converter and decrease the efficiency of the system, but it can significantly reduce the weight and volume of the power conversion system and minimize grid isolation issues. In 2010, Lu et al. [22, 23] proposed a planar high-frequency transformer-based PV inverter system as shown in Fig. 2.30. Higher output power from multiple PV arrays can be achieved by connecting each PV array to its own DC to AC converter and single-phase transformer. The primaries of the high-frequency transformer links are connected in an open delta energized by high-frequency voltage from DC to AC converters, where the converter

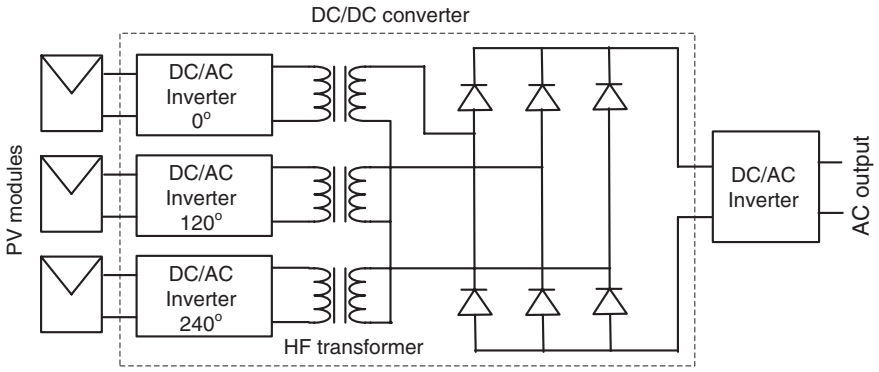

Fig. 2.30 High-frequency (*HF*) transformer-based PV inverter power circuit

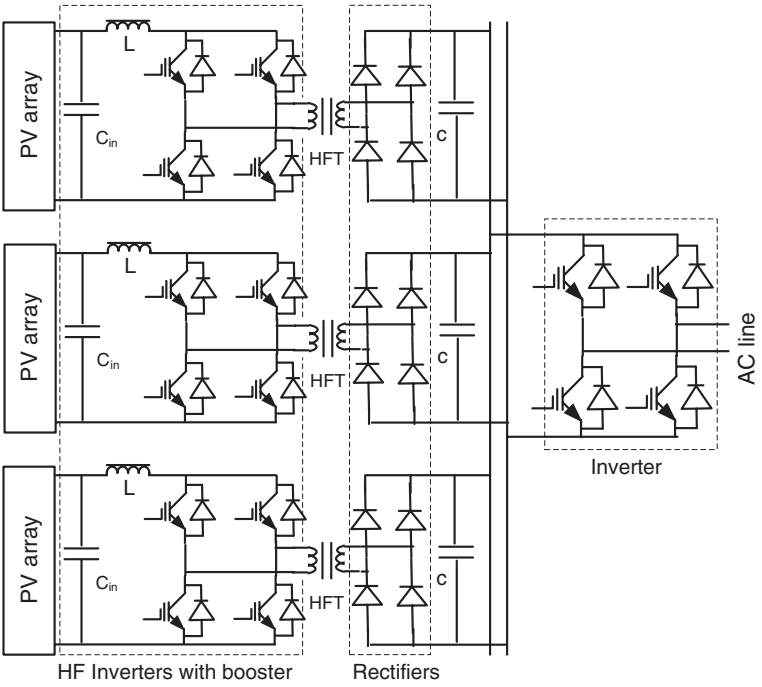

Fig. 2.31 High-frequency transformer (*HFT*)-based PowerLynx Powerlink PV 4.5 kW inverter

output voltages are phase shifted each other by 120°. The secondaries of the high-frequency transformer links are connected in a wye configuration, and the output is connected to a 50 or 60 Hz DC to AC converter through a high-frequency three-phase rectifier. The detailed design and analysis of the HF planar transformer were reported in [24, 25]. The Original Equipment Manufacturer commercially developed the high-frequency transformer-based three-string PV inverter, PowerLynx Powerlink PV 4.5 kW, as shown in Fig. 2.31 [26].

2.3.3 Single-Stage Solar PV Inverter for Small-Scale Systems

Compared to the single-stage one, the multistage power conversion is somewhat more expensive and affects the efficiency of the PV inverter. In order to reduce the volume and weight as well as the power conversion loss and cost, a hybrid PV-battery-powered DC bus system was proposed in 2009 [27]. The DC to AC conversion stage-less DC bus system is very applicable to electronic equipment and appliances with high system efficiencies. The PV-battery-powered DC bus system

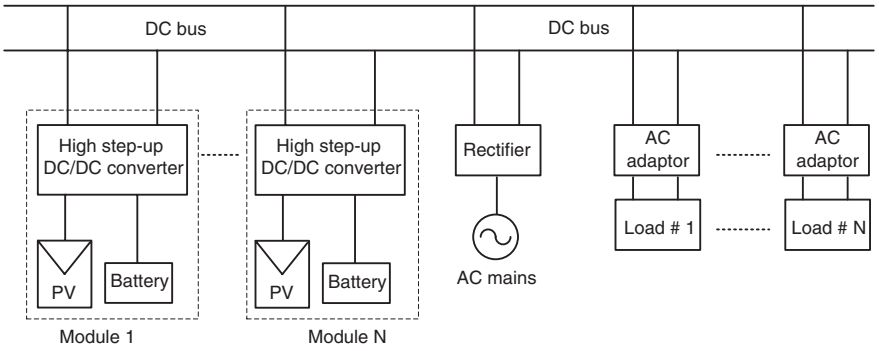

Fig. 2.32 PV-battery-powered DC bus system

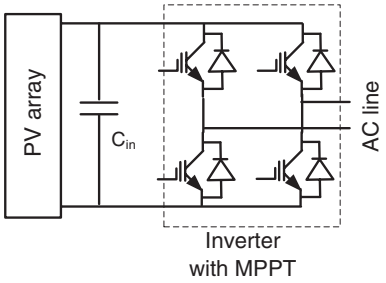

Fig. 2.33 Full-bridge with MPPT-based circuit topology of single-stage inverter

is shown in Fig. 2.32. For AC systems, a single-stage PV inverter was proposed in [28], and the circuit topology of single-stage inverter is shown in Fig. 2.33.

The proposed inverter performs a dual function: MPPT and outputting a sinusoidal current, which makes the control circuit complex. In [29], an alternative control technique was developed to reduce the complexity of the control circuit. However, the common-mode issue was not considered in the proposed single-stage inverter systems. The neutral point clamped (NPC) converter topology has the opportunity to connect the grid neutral point to middle point of the DC link, reducing the ground leakage currents. In this context, an NPC topology-based single-phase PV inverter as shown in Fig. 2.34 was presented in [30] and a three-phase PV inverter system in Fig. 2.35 was implemented in [31]. Since the presented circuits are run as buck converters, the PV array voltages should be greater than the peak values of the output AC voltages. If V_{rms} is the inverter output AC voltage and R *is* the reservation factor, the minimum array voltage can be calculated as

$$V_{\text{A}} = \sqrt{2} V_{\text{rms}} R. \tag{2.13}$$

Therefore, a few PV arrays in series connection are necessary to obtain the desired voltage. From the available literature, several single-stage topologies have been proposed based on either boost or buck–boost configurations. An integrated

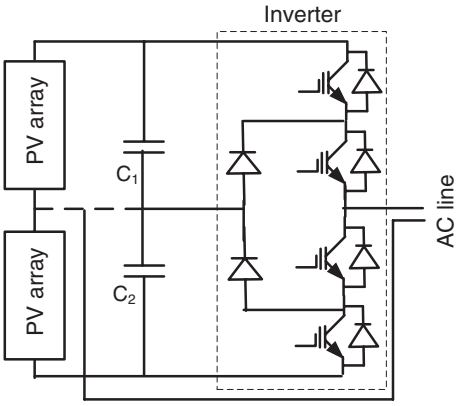

Fig. 2.34 Circuit topology of single-stage inverter: NPC with grid neutral connected to the middle point of DC link

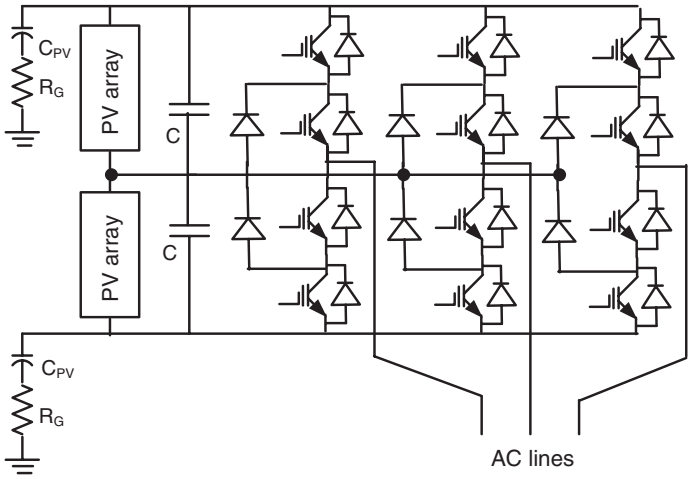

Fig. 2.35 NPC topology-based three-phase PV inverter

(boost converter and full-bridge inverter) PV inverter circuit topology shown in Fig. 2.36 was presented in [32]. The output power quality and the efficiency of the inverter are limited by the fact that the boost converter cannot generate the output voltage lower than the input voltage. A universal single-stage PV inverter shown in Fig. 2.37 was presented in [33] that can operate as a buck, boost, or buck–boost converter. This inverter can operate with a wide range of input voltage, improving the power quality and the efficiency. Using the integrated buck–boost and inversion functions, several modified configurations have been presented in [34, 35]. However, these topologies are only suitable for small-scale (e.g., <100 kW) PV systems, where the PV array normally interconnects with a low-voltage public network.

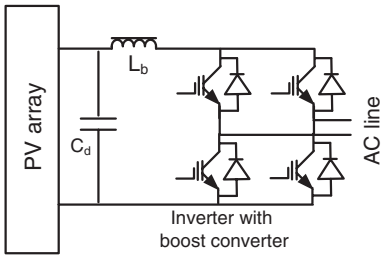

Fig. 2.36 Single-stage power circuit with boost converter

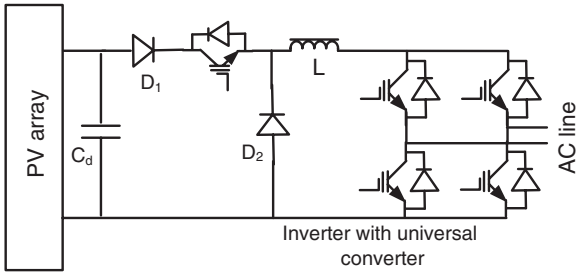

Fig. 2.37 Single-stage power circuit with universal converter

2.3.4 ABB and Siemens Solar PV Inverters for Small-Scale Systems

Although the galvanic isolation is not a requirement in Germany in the low-voltage public network, a residual current monitoring unit needs to be installed for the grid connection of transformer-less PV inverters. Most standards (e.g., IEEE 1547, EN 61000-3-2, and IEC 61727) allow the DC current injection to vary between 0.5 and 1 % of the rated current [36]. Therefore, the transformer-less inverter system should have some extra protective devices to ensure the safety issues. ABB is one of the leading manufacturers of PV inverters. In order to interconnect the PV array to the public electricity network, ABB developed the transformer-less single-phase string PV inverter model PVS300, suitable for small-scale PV systems (i.e., 3.3–8.0 kW). The PVS300 inverter converts the DC generated by PV arrays at a voltage ranging 335–800 V into single-phase 230 V AC that can be fed into the public network through protective devices as shown in Fig. 2.38 [37]. Due to the high content of harmonics in the output power and the use of high switching frequency of switching devices, the system consists of a heavy filter circuit and electromagnetic interference (EMI) filter, which may increase the losses and cost of the system.

The SINVERT PVM inverters are transformer-less, 3-phase PV inverters developed by Siemens, to convert solar DC energy at a voltage ranging in 380–850 V into 3-phase 400 V AC voltage for feeding into public electricity network. SINVERT PVM inverters are available with power outputs from 10 to 20 kW. The PV array

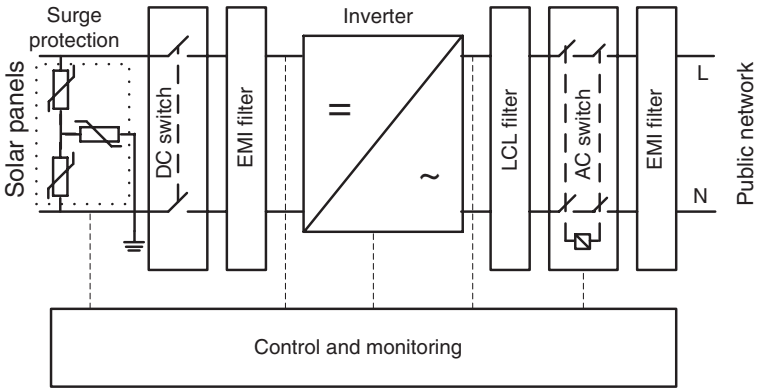

Fig. 2.38 ABB PVS300 string inverter design and grid connection

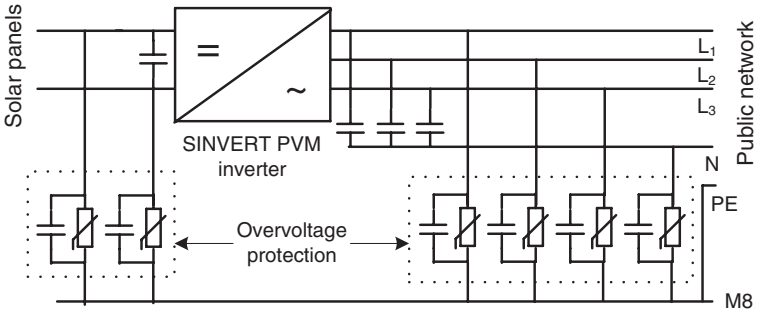

Fig. 2.39 Siemens SINVERT PVM string inverter design and grid connection

interconnection to utility grid through SINVERT inverter with safety devices is shown in Fig. 2.39 [38].

2.4 Medium- and Large-Scale Solar PV Systems

For medium- and large-scale solar PV electricity generation, there are two well-established inverter technologies: the centralized and string technologies as shown in Figs. 2.40 and 2.41, respectively.

In the centralized PV inverter technology, each string consists of a series of PV modules to reach the voltage requirement without amplification and then a few strings are parallel connected to a common inverter circuit. The number of strings mainly depends on the power levels. This technology eliminates the amplification stage, but possesses some major limitations, such as voltage mismatch loss

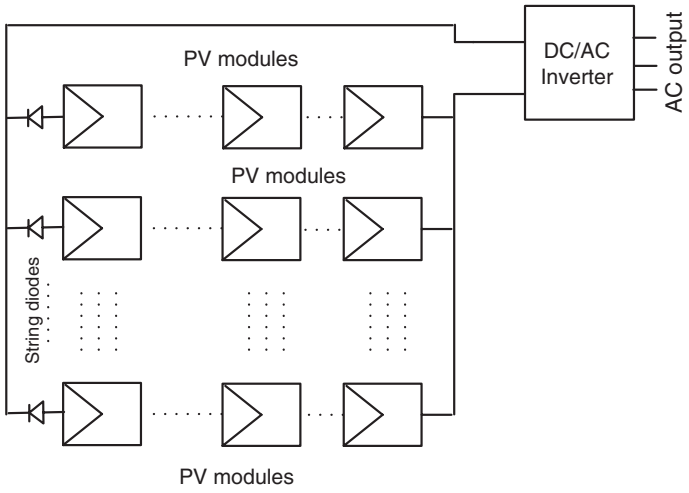

Fig. 2.40 Centralized PV inverter topology

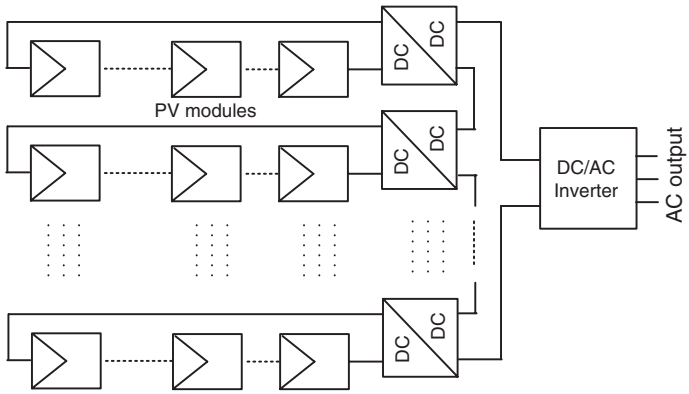

Fig. 2.41 String PV inverter topology

between PV modules and power losses due to common MPPT [26]. In order to control every string individually, the string technology uses a DC to DC converter for each string, which improves the system efficiency. In order to minimize the voltage mismatch in the strings, a battery-integrated boost converter was proposed to eliminate the voltage regulation stage [39]. The block diagram of battery-integrated boost converter is shown in Fig. 2.42, and the proposed converter-based PV inverter system is shown in Fig. 2.43. The detailed analysis of the proposed converter is presented in [40].

The ABB central inverters are especially designed for medium-scale PV power plants. The PVS800 version is a 3-phase inverter with a power capacity in the

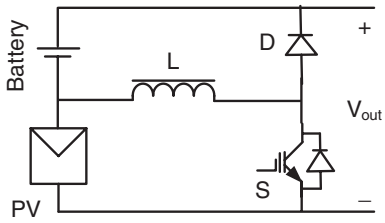

Fig. 2.42 Battery-integrated boost converter

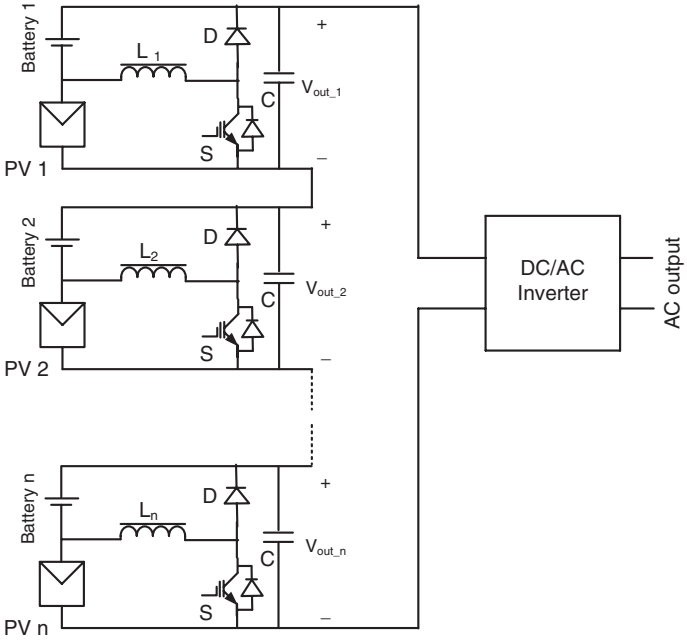

Fig. 2.43 Battery-integrated boost converter-based PV inverter system

range of 100–500 kW. The PVS800 inverter topology allows a parallel connection directly on the AC side, for grid connection through a step-up power frequency transformer [41]. The transformer steps up the inverter output voltage from 300 V AC to grid voltage level (e.g., 6–36 kV). The central inverter design and grid connection are depicted in Fig. 2.44. ABB has been delivering worldwide vacuum cast coil dry-type transformers for PV applications. The cast coil dry-type transformers are non-flammable and moisture proof. They feature a solid isolation system which is discharge-free. However, the volume and weight of a 0.4/36 kVA, 1 MVA vacuum cast coil transformer are about 4.3 m^3 and 3,250 kg, respectively, and no-load and full-load losses are 3.1 and 11.5 kW, respectively [42]. Moreover, dry-type transformers can be sensitive to water, microcracks, temperature variations,

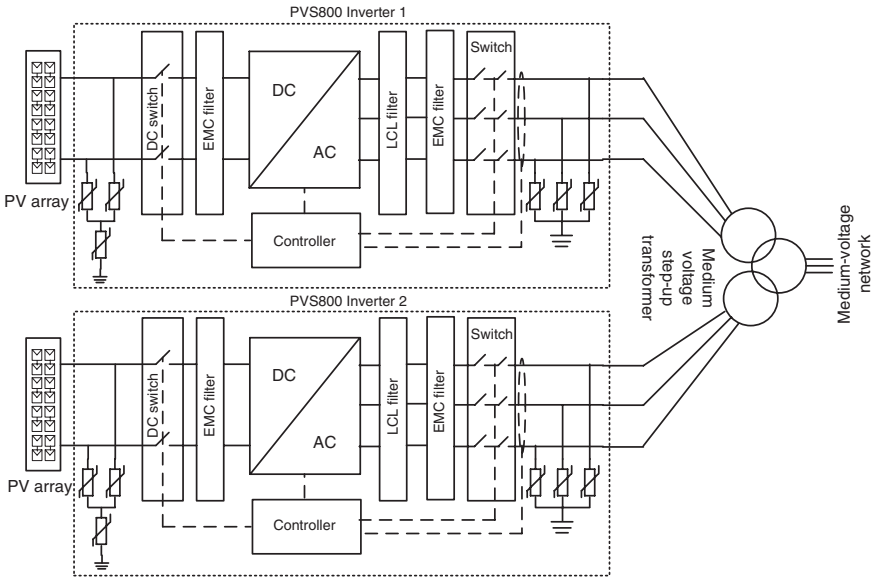

Fig. 2.44 ABB central inverter design and medium-voltage (*MV*) grid connection

and pollution which can block cooling ducts. Due to the use of traditional two-level inverter, the harmonic content in the output power is high. Usually, high-frequency pulse-width-modulated (PWM) gate signals are used to drive switching devices to reduce the harmonic content. Due to high-harmonic content and high-frequency stitching, the system requires a heavy LCL filter circuit and an electromagnetic compatibility (EMC) filter, which may increase the losses and cost of the system.

Besides its low-voltage system, Siemens also developed the SINVERT PVS inverter-based system for medium-scale PV plants. The AC output voltage and power capacity of PVS version inverters are in the range of 288–370 V and 500–630 kW, respectively, as summarized in Table 2.2. The 1–2.52 MW central inverters were designed by paralleling 2–4 PVS inverters through transformer and switchgear at the grid side. The design and grid connection of 2-inverters-based system is illustrated in Fig. 2.45 [43]. Siemens developed GEAFOL cast–resin transformers for grid connection of PV arrays. With GEAFOL, it is possible to avoid the limitations associated with liquid-filled transformers while retaining the

Table 2.2 Capacity of PVS version inverters

Versions	PVS500	PVS585	PVS600	PVS630
AC output voltage (V)	288	340	370	370
Power capacity (kW)	500	585	600	630
Min. input voltage (V)	450	530	570	570

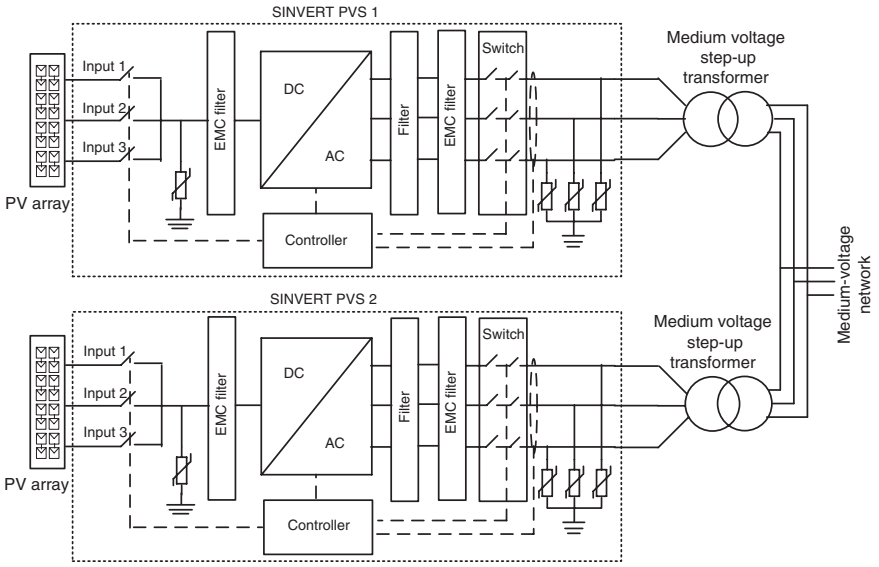

Fig. 2.45 Siemens central inverter design and medium-voltage grid connection

properties such as operational safety, resistance to humidity, mechanical strength, and compact design. However, no-load and full-load losses of a 0.4/30 kV, 1 MVA GEAFOL transformer are about 3.1 and 10 kW, respectively, and the volume and weight are about 3.5 m^3 and 2,990 kg, respectively [44].

Although these special transformers are compact compared with conventional distribution transformers, they are still large and heavy for PV applications. The large-size and heavy-step-up transformer may increase the system weight and volume and can be expensive and complex for installation and maintenance. The medium-voltage inverter may be the best possible solution to interconnect the PV array to the medium-voltage grid directly. Moreover, electrical isolation is important for the interconnection of the medium-voltage grid and PV array. Since the installation of large-scale PV power plants started commercially in 2007, the medium-voltage inverter for interconnection of PV systems has been attracting great attention.

In 2011, different MV multilevel inverter topologies were compared for the possible medium-voltage grid connection of wind turbine and PV systems [45, 46]. The modular multilevel cascaded (MMC) topology was considered as a possible candidate for medium-voltage inverter systems. The MMC inverter requires multiple isolated and balanced DC sources. In [47], a medium or HF link was proposed to generate multiple isolated and balanced DC sources for the MMC from a single source and in [48], a medium-frequency transformer link was developed to verify the feasibility of the new concept of voltage step-up using the MMC inverters. Compared with the conventional transformers operated at the power frequency (50

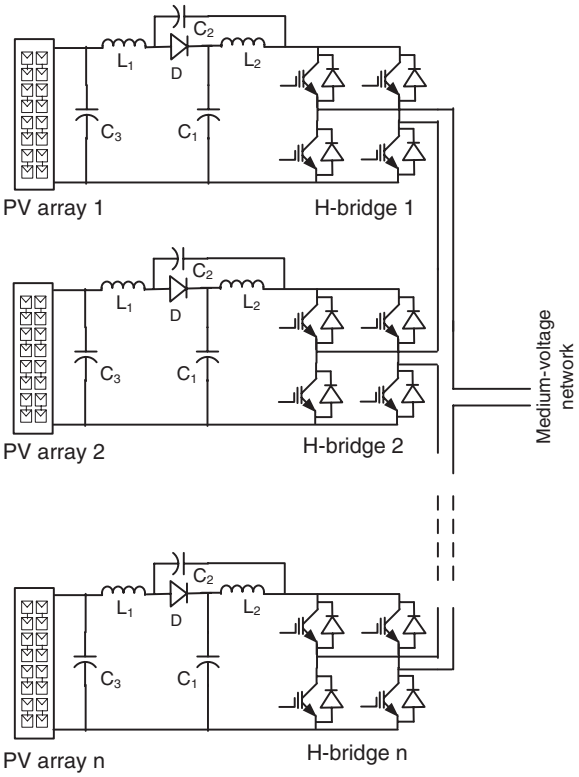

Fig. 2.46 Quasi-Z source converter-based medium-voltage PV inverter (one of 3 phases)

or 60 Hz), the medium-frequency transformer link has much smaller and lighter magnetic cores and windings and thus much lower costs.

In 2012, by combining a quasi-Z source inverter into an MMC as shown in Fig. 2.46, a medium-voltage PV inverter was proposed in [49].

The proposed inverter does not have isolation between PV array and medium-voltage grid. Multiphase isolated DC to DC converter-based MMC inverter topology as shown in Fig. 2.47 was proposed in [50, 51]. In the proposed configuration, the voltage balancing is the challenging issue, since each H-bridge cell is connected to a PV array through a DC to DC converter. A common DC link may be one of the possible solutions to minimize the voltage imbalance problem, and a single DC-link-based inverter in Fig. 2.48 was presented in [52, 53]. Although this design may reduce the voltage balancing problem in the grid side, the generation of common DC-link voltage from different PV arrays makes the inverter operation complex and limits the range of MPPT operation.

As an alternative approach to minimize the voltage imbalance problem with a wide range of MPPT operation, a common magnetic link was proposed [3]. The boost converter is considered for the MPPT operation. The array DC power is converted to a high-frequency AC through a high-frequency inverter. The inverter also

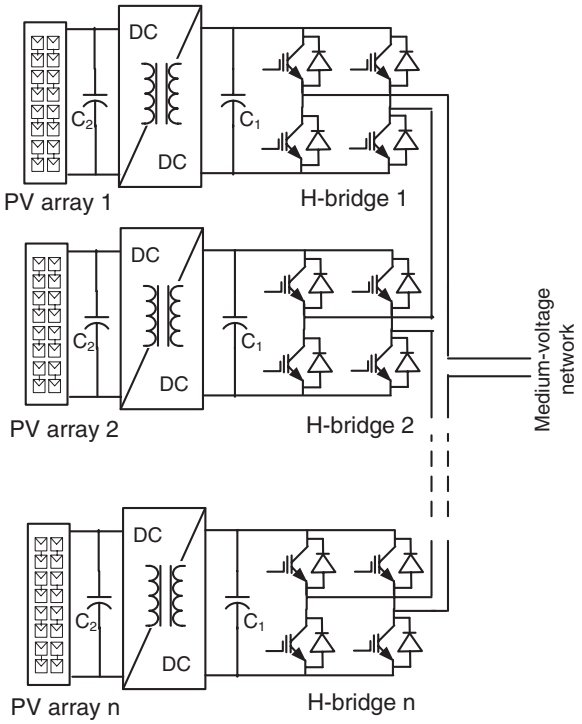

Fig. 2.47 Multiphase isolated converter-based medium-voltage PV inverter (one of 3 phases)

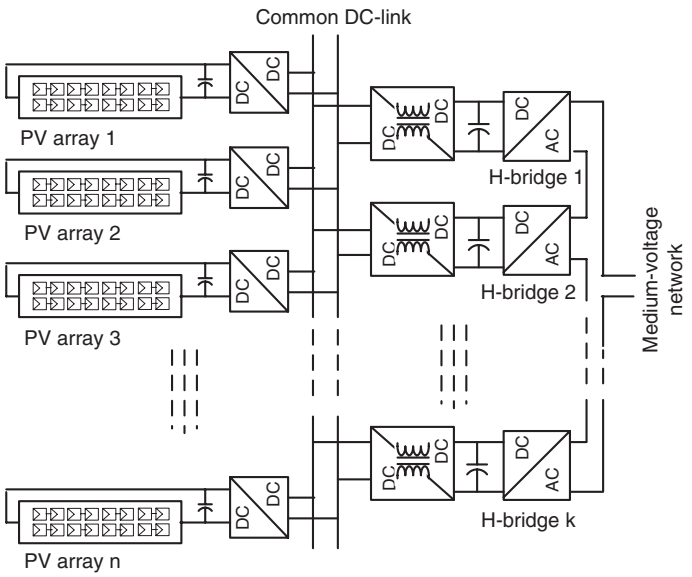

Fig. 2.48 Common DC-link-based medium-voltage PV inverter (one of 3 phases)

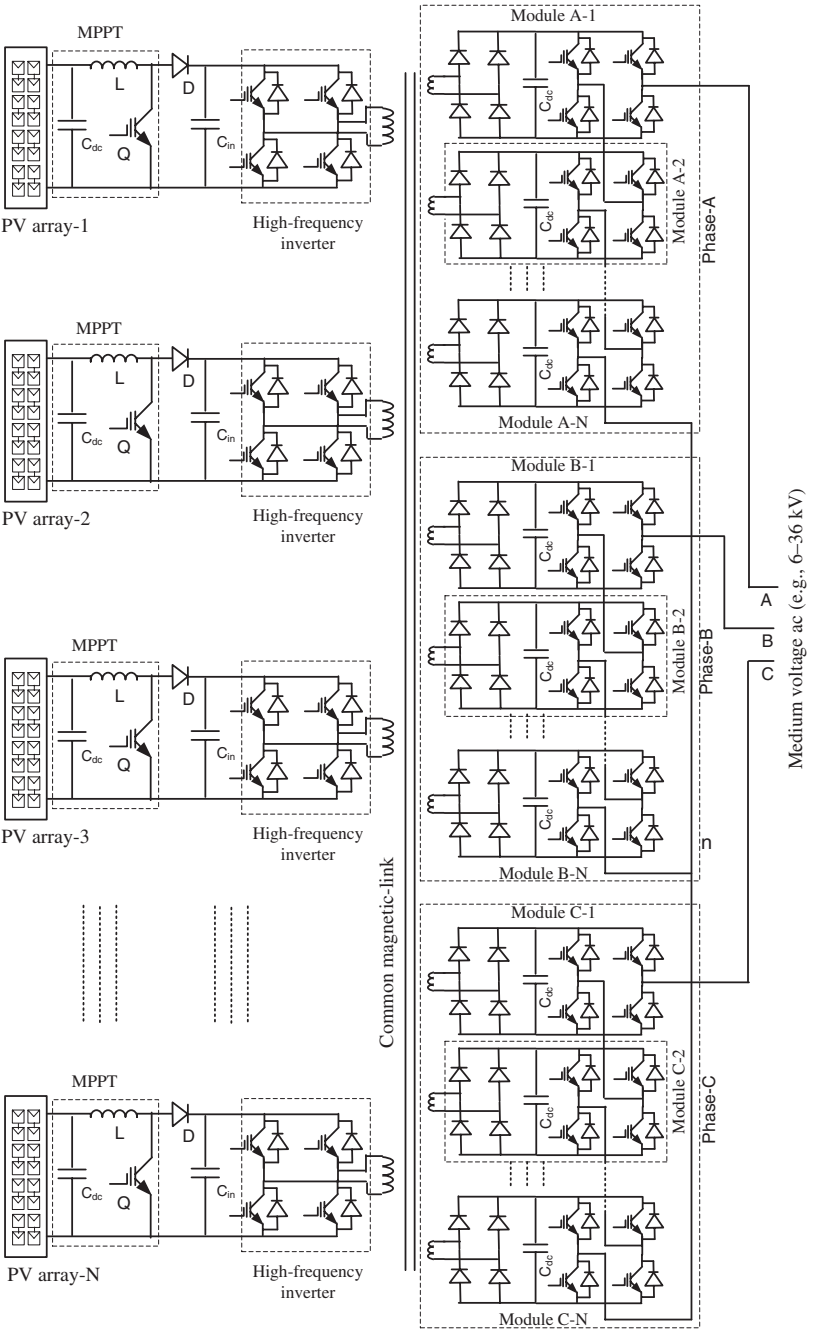

Fig. 2.49 Common magnetic-link-based 3-phase medium-voltage PV inverter

ensures constant output voltage. The inverter is connected to a primary winding of a multiwinding high-frequency magnetic link. Each secondary winding works as an isolated source and is connected to an H-bridge cell through a bridge rectifier. The number of primary windings depends on the number of PV arrays, and the number of secondary windings depends on number of levels of the inverter. The detailed power circuit of common magnetic-link-based PV inverter system is shown in Fig. 2.49 [3]. In medium- or large-scale PV power plants, several PV arrays are operated in parallel. The multiple-input multiple-output magnetic link can incorporate the parallel operation of multiple PV arrays, where each PV array is connected to a primary winding through a booster and high-frequency inverter [54]. The magnetic link also provides electrical isolation between the PV array and the grid, which can thus inherently overcome the common-mode and voltage imbalance problems and ensure a wide range of MPPT operation and safety of operating personnel.

2.5 Summary

Besides the traditional systems, which require a step-up transformer to connect the renewable generation systems to the grid, many other recently proposed converter topologies for step-up-transformer-less direct grid interconnection are also reviewed in detail with the aim of presenting a complete picture of power converter systems. In order to develop a common converter for both the wind and PV power generation systems, appropriate converter topologies should be investigated. In this chapter, most of the existing power converters are reviewed. In order to reduce the system volume and weight as well as to improve the efficiency, a number of transformer-less single-stage inverter topologies have been proposed in the past decades for small-scale PV power generation systems. The common-mode or leakage current and personal safety are really critical issues with these inverter systems. Most of the commercially available system uses the traditional two-level inverter in which the switching devices are driven by high-frequency PWM gate signals. Due to high-harmonic contents and high-frequency switching, the system requires a heavy LCL filter circuit and an EMC filter, which may increase the losses and cost of the system.

Today, the industrial trend is to move away from these heavy and large-size passive components to compact and lightweight systems that use more and more semiconductor devices in modular construction. It is found that multilevel converters with medium-frequency links would be a feasible option to develop a MV converter for the direct grid integration of PV power plants. Although different multilevel converter topologies have been developed in the last few decades, most of them are not suitable for medium-voltage applications. Because of some special features, such as the number of components scaling linearly with the number of levels, and the identical individual modules of completely modular construction enabling high-level number attainability, the MMC converter topology is

considered as a highly feasible candidate for medium-voltage applications. The MMC converter requires multiple isolated and balanced DC sources. The medium-frequency magnetic link may be the best option to generate multiple isolated and balanced DC sources for the MMC inverter from a single power source. Compared with the power frequency transformers, the medium-frequency links have much smaller and lighter magnetic cores and windings and thus much lower costs.

References

1. Earth policy institute Climate, energy and transportation, world cumulative wind turbine installations [online]. Available at: http://www.earth-policy.org. Accessed on 25 Mar 2013
2. Islam MR, Guo YG, Zhu JG (2012) 11-kV series-connected H-bridge multilevel converter for direct grid connection of renewable energy systems. J Int Conf Elec Mach Syst 1(2):211–219
3. Islam MR, Guo YG, Zhu JG (2014) A multilevel medium-voltage inverter for step-up-transformer-less grid connection of photovoltaic power plants. IEEE J Photovoltaics 4(3):881–889
4. Islam MR, Guo YG, Zhu JG (2014) A high-frequency link multilevel cascaded medium-voltage converter for direct grid integration of renewable energy systems. IEEE Trans Power Electron 29(8):4167–4182
5. Islam MR, Guo YG, Lin ZW, Zhu JG (2014) An amorphous alloy core medium frequency magnetic-link for medium voltage photovoltaic inverters. J Appl Phys 115(17):17E710-1–17E710-3
6. Sharma VK, Colangelo A, Spagna G (1995) Photovoltaic technology: basic concepts, sizing of a standalone photovoltaic system for domestic applications and preliminary economic analysis. Energy Convers Manage 36(3):161–174
7. Santos JL, Antunes F, Chehab A, Cruz C (2006) A maximum power point tracker for PV systems using a high performance boost converter. Sol Energy 80(7):772–778
8. Hua C, Shen C (1998) Study of maximum power tracking techniques and control of DC/DC converters for photovoltaic power system. In: 29th annual IEEE power electronics specialists conference, Fukuoka, Japan, 17–22 May 1998, pp 86–93
9. Jaboori MG, Saied MM, Hanafy AAR (1991) A contribution to the simulation and design optimization of photovoltaic systems. IEEE Trans Energy Conversion 6(3):401–406
10. Bose BK, Szczesny PM, Steigerwald RL (1985) Microcomputer control of a residential photovoltaic power conditioning system. IEEE Trans Ind Appl 21(5):1182–1191
11. Islam MR, Islam MR, Beg MRA (2008) Renewable energy resources and technologies practice in Bangladesh. Renew Sustain Energy Rev 12(2):299–343
12. Islam MR, Guo YG, Zhu JG, Jin J (2011) Design and fabrication of a microcontroller based maximum power point tracker for renewable energy systems. J Appl Supercond Electromagnet 2(1):17–23
13. Islam MR, Guo YG, Zhu JG, Rabbani MG (2010) Simulation of PV array characteristics and fabrication of microcontroller based MPPT. In: 6th international conference on electrical and computer engineering (ICECE), Dhaka, Bangladesh, 18–20 Dec, pp 155–158
14. Sugimoto H, Dong H (1997) A new scheme for maximum photovoltaic power tracking controls. In: Power conversion conference, Nagaoka, Japan, 3–6 Aug 1997, pp 691–696
15. Ogura K, Nishida T, Hiraki E, Nakaoka M, Nagai S (2004) Time-sharing boost chopper cascaded dual mode single-phase sinewave inverter for solar photovoltaic power generation system. In: IEEE 35th annual power electronics specialists conference, Aachen, Germany, 20–25 June 2004, pp 4763–4767
16. Young-Ho K, Jun-Gu K, Young-Hyok J, Chung-Yuen W, Yong-Chae J (2010) Photovoltaic parallel resonant DC-link soft switching inverter using hysteresis current control. In:

Twenty-fifth annual IEEE applied power electronics conference and exposition, Palm Springs, Canada, 21–25 Feb 2010, pp 2275–2280
17. Nema S, Nema RK, Agnihotri G (2011) Inverter topologies and control structure in photovoltaic applications: a review. J Renew Sustain Energy 3(1):012701-1–012701-23
18. Patrao I, Figueres E, Espin FG, Garcera G (2011) Transformerless topologies for grid-connected single-phase photovoltaic inverters. Renew Sustain Energy Rev 15(7):3423–3431
19. Rahman MF, Zhong L (1997) A new, transformerless, photovoltaic array to utility grid interconnection. In: 1997 international conference on power electronics and drive systems, Singapore, 26–29 May 1997, pp 139–143
20. SMA Solar Technology AG. Sunny Boy 5000TL multi-string inverter [online]. Available at: http://www.sma.de. Accessed on 25 Feb 2013
21. Agheb E, Bahmani MA, Hoidalen HK, Thiringer T (2012) Core loss behavior in high frequency high power transformers-II: arbitrary excitation. J Renew Sustain Energy 4(3):033113-1–033113-11
22. Lu J, Stegen S, Butler D (2010) High frequency and high power density transformers for DC/DC converter used in solar PV system. In: 2010 2nd IEEE international symposium on power electronics for distributed generation systems, Hefei, China, 16–18 June 2010, pp 481–484
23. Lu J, Butler D (2011) High frequency transformers for DC/DC converter used in solar PV system. J Energy Power Eng 5:536–541
24. Lu J, Dawson F (2011) Characteristics for high frequency planar transformer with a novel comb-shaped shield. IEEE Trans Magn 47(10):4493–4496
25. Panchal C, Lu J (2011) High frequency planar transformer for universal contact-less battery charging platform. IEEE Trans Magn 47(10):2764–2767
26. Kjaer SB, Pedersen JK, Blaabjerg F (2005) A review of single-phase grid-connected inverters for photovoltaic modules. IEEE Trans Ind Appl 41(5):1292–1306
27. Lu DDC, Agelidis VG (2009) Photovoltaic-battery-powered DC bus system for common portable electronic devices. IEEE Trans Power Electron 24(3):849–855
28. Liang TJ, Kuo YC, Chen JF (2001) Single-stage photovoltaic energy conversion system. IEE Proc Electric Power Appl 148(4):339–344
29. Chen Y, Smedley KM (2004) A cost-effective single-stage inverter with maximum power point tracking. IEEE Trans Power Electron 19(5):1289–1294
30. Gonzalez R, Gubia E, Lopez J, Marroyo L (2008) Transformerless single-phase multilevel-based photovoltaic inverter. IEEE Trans Ind Electron 55(7):2694–2702
31. Cavalcanti MC, Farias AM, Olivetra KC, Neves FAS, Afonso J (2012) Eliminating leakage currents in neutral point clamped inverters for photovoltaic systems. IEEE Trans Ind Electron 59(1):435–443
32. Junior LG, Brito MAGD, Sampaio LP, Canesin CA (2011) Single stage converters for low power stand-alone and grid-connected PV systems. In: 2011 IEEE international symposium on industrial electronics, Gdansk, Poland, 27–30 June 2011, pp 1112–1117
33. Prasad BS, Jain S, Agarwal V (2008) Universal single-stage grid-connected inverter. IEEE Trans Energy Conversion 23(1):128–137
34. Wang C (2004) A novel single-stage full-bridge buck-boost inverter. IEEE Trans Power Electron 19(1):150–159
35. Patel H, Agarwal V (2009) A single-stage single-phase transformer-less doubly grounded grid-connected PV interface. IEEE Trans Energy Conversion 24(1):93–101
36. Meneses D, Blaabjerg F, García O, Cobos JA (2013) Review and comparison of step-up transformerless topologies for photovoltaic AC-module application. IEEE Trans Power Electron 28(6):2649–2663
37. ASEA Brown Boveri (ABB). Solar photovoltaic string inverter [online]. Available at: http://www.abb.com. Accessed on 13 May 2013
38. SIEMENS. SINVERT PVM operating instruction 07/2010 [online]. Available at: http://www.siemens.com/. Accessed on 13 April 2014
39. Du Y, Lu DDC (2010) Analysis of a battery-integrated boost converter for module-based series connected photovoltaic system. In: 2010 international power electronics conference, Sapporo, Japan, 21–24 June 2010, pp 694–698

40. Du Y, Lu DDC (2011) Battery-integrated boost converter utilizing distributed MPPT configuration for photovoltaic systems. Sol Energy 85(9):1992–2002
41. ASEA Brown Boveri (ABB). Solar photovoltaic central inverter [online]. Available at: http://www.abb.com. Accessed on 10 Mar 2014)
42. Islam MR, Guo YG, Zhu JG (2014) A review of offshore wind turbine nacelle: technical challenges, and research and developmental trends. Renew Sustain Energy Rev 33:161–176
43. SIEMENS. SINVERT PVS solar photovoltaic inverter [online]. Available at: http://www.siemens.com/. Accessed on 13 Feb 2014)
44. ASEA Brown Boveri (ABB). GEAFOL transformer [online]. Available at: http://www.abb.com. Accessed on 02 July 2013)
45. Islam MR, Guo YG, Zhu JG (2011) Performance and cost comparison of NPC, FC and SCHB multilevel converter topologies for high-voltage applications. In: 2011 international conference on electrical machines and systems, Beijing, China, 20–23 Aug 2011, pp 1–6
46. Islam MR, Guo YG, Zhu JG, Dorrell (2011) Design and comparison of 11 kV multilevel voltage source converters for local grid based renewable energy systems. In: Proceedings of the 37th annual conference on IEEE industrial electronics society, Melbourne, Australia,7–10 Nov 2011, pp 3596–3601
47. Islam MR, Guo YG, Zhu JG (2011) H-bridge multilevel voltage source converter for direct grid connection of renewable energy systems. In: 2011 IEEE PES innovative smart grid technologies Asia (ISGT), Perth, Australia, 13–16 Nov 2011, pp 1–7
48. Islam MR, Guo YG, Zhu JG (2013) A medium-frequency transformer with multiple secondary windings for medium-voltage converter based wind turbine generating systems. J Appl Phys 113(17):17A324-1–17A324-3
49. Sun D, Ge B, Peng FZ, Haitham AR, Bi D, Liu Y (2012) A new grid-connected PV system based on cascaded H-bridge quasi-Z source inverter. In: 2012 IEEE international symposium on industrial electronics, Hangzhou, China, 28–31 May 2012, pp 951–956
50. Choi H, Zhao W, Ciobotaru M, Agelidis VG (2012) Large-scale PV system based on the multiphase isolated DC/DC converter. In: 3rd IEEE international symposium on power electronics for distributed generation systems, Aalborg, Denmark, 25–28 June 2012, pp 801–807
51. Zhao W, Choi H, Konstantinou G, Ciobotaru M, Agelidis VG (2012) Cascaded H-bridge multilevel converter for large-scale PV grid-integration with isolated DC-DC stage. In: 3rd IEEE international symposium on power electronics for distributed generation systems, Aalborg, Denmark, 25–28 June 2012, pp 849–856
52. Kouro S, Fuentes C, Perez M, Rodriguez J (2012) Single DC-link cascaded H-bridge multilevel multistring photovoltaic energy conversion system with inherent balanced operation. In: 38th annual conference on IEEE industrial electronics society, Montreal, QC, Canada, 25–28 Oct 2012, pp 4998–5005
53. Rivera S, Wu B, Kouro S, Wang H, Zhang D (2012) Cascaded H-bridge multilevel converter topology and three-phase balance control for large scale photovoltaic systems. In: 3rd IEEE international symposium on power electronics for distributed generation systems, Aalborg, Denmark, 25–28 June 2012, pp 690–697
54. Islam MR, Lei G, Guo YG, Zhu JG (2014) Optimal design of high-frequency magnetic-links for power converters used in grid connected renewable energy systems. IEEE Trans Magn. doi:10.1109/TMAG.2014.2329939

http://www.springer.com/978-3-662-44528-0

Power Converters for Medium Voltage Networks

Islam, M.R.; Guo, Y.; Zhu, J.

2014, XLI, 278 p. 356 illus., 70 illus. in color., Hardcover
ISBN: 978-3-662-44528-0